Teleseismic traveltimes, topography and the lithospheric structure across central Mongolia

Carole Petit, Christel Tiberi, Anne Deschamps, Jacques Déverchère

GEOPHYSICAL RESEARCH LETTERS, VOL. 35, L11301, doi:10.1029/2008GL033993, 2008

Teleseismic traveltimes, topography and the lithospheric structure across central Mongolia

Carole Petit,[1] Christel Tiberi,[1] Anne Deschamps,[2] and Jacques Déverchère[3]

Received 20 March 2008; revised 24 April 2008; accepted 30 April 2008; published 14 June 2008.

[1] Teleseismic travel times recorded along a 1000 km-long, ∼N-S transect across central Mongolia are used together with topography and gravity data to constrain the deep lithospheric structure of this region. Time residuals appear positively correlated with the topography, suggesting that P-wave velocity changes correspond to density variations which in turn cause an isostatic uplift of the topography. Using a simple local isostasy model and a Monte-Carlo inversion for the crust and asthenosphere velocities and density/velocity conversion factors, we determine best-fitting Moho and lithosphere-asthenosphere boundary (LAB) geometries which satisfyingly reproduce the observed topography and gravity data. The model is validated using previously published 1D S-wave velocity models obtained from receiver function analyses. Our results indicate that most of the long-wavelength topography is supported by the asthenosphere buoyancy. The Hangai dome, in the southern half of the transect, appears mainly supported by a rather shallow (60–70 km) asthenospheric uplift, whereas the Siberian platform at the extreme north of the profile is underlain by a very thick (∼200 km) lithosphere. Misfits to the observed Bouguer gravity anomaly occur near major faults, probably because of lithospheric flexure. **Citation:** Petit, C., C. Tiberi, A. Deschamps, and J. Déverchère (2008), Teleseismic traveltimes, topography and the lithospheric structure across central Mongolia, *Geophys. Res. Lett.*, *35*, L11301, doi:10.1029/2008GL033993.

1. Introduction

[2] In continental domains, topography results from a combination of tectonic activity inducing crustal thickening or thinning and flexure, and sub-lithospheric processes, for example asthenosphere up- or down-welling. In turn, isostasy implies that the deep structures of the lithosphere, i.e., the Moho and lithosphere-asthenosphere boundary (LAB) geometries are somewhat reflected in the topography. The geometry of these interfaces also influences the gravity signal and the travel time of seismic rays. The correlation between Bouguer gravity and topography has long been used to infer the flexural wavelength of the lithosphere [*Forsyth*, 1985]. At a regional scale, forward modeling of gravity and topography has been used for distinguishing the relative roles of sub-lithospheric and crustal thickening processes in the topography genesis [e.g., *Petit et al.*, 2002; *Missenard et al.*, 2006]. Gravity and teleseismic travel time residuals can also be inverted to retrieve the deep density and velocity structures [*Tibéri et al.*, 2003]. Seismic tomography, gravity and topography data have been used at a global scale for similar purposes [e.g., *Kaban et al.*, 2004]. Yet, up to now, no attempt has been done to evaluate how teleseismic travel times and topography are correlated at a regional scale.

[3] In this paper, we present the results of a joint teleseismic, topography and gravity modeling to infer the lithospheric structure along a ∼NS transect of 19 seismic stations in central Mongolia (Figure 1). This region is characterized by active transpressional tectonics causing mountain building in its northern and southern areas (Sayan Mountains and Gobi-Altai range, respectively [e.g., *Arjannikova et al.*, 2004; *Cunningham*, 2005; *Vassallo et al.*, 2007]) and by a wide central topographic dome of enigmatic origin, the Hangai Dome [e.g., *Cunningham*, 2001] (Figure 1). From the analysis of gravity and topography data, *Petit et al.* [2002] have inferred an asthenospheric origin for the uplift Hangai dome but their model lacked independent constraints on the depth and density contrast associated with the LAB.

2. MOBAL Experiment

[4] The MOBAL seismic experiment took place in a French-Mongolian-Russian collaborative work in 2003. A temporary network of 3-component seismic stations was deployed in a 1000 km long roughly N-S transect between Siberia and Mongolia (Figure 1). The transect runs from the Siberian platform through the Sayan-Baikal mountains, the Hangai Dome and ends up at the Gobi-Altai range (Figure 1). This profile comprises 19 broadbandseismic stations continuously recording at 32.5 or 40 samples per second from April to October 2003. The average station spacing is ∼50–100 km.

[5] The purpose of this seismic experiment is to use passive teleseismic events to obtain information about the lithospheric structure of Mongolia. We focus this study on the relation between travel time residuals and topography to deduce the geometry of the main boundaries within the 200 first kilometers: the Moho discontinuity, and the lithosphere-asthenosphere boundary.

[6] We select 82 teleseismic events with good signal to noise ratio and with a clear first P-wave onset. These events have epicentral distances ranging between 30° and 90°, and mainly come from the Pacific subductions. We obtain the travel time residuals by subtracting the theoretical travel time calculated from IASP91 model [*Kennett and Engdahl*, 1991] from the observed P-wave arrival time. To get rid of errors coming from event mislocation, original time and deep mantle sources, we remove the mean of all travel times for a given event. That leads us with relative travel times

[1] Laboratoire de Tectonique, CNRS-UPMC, Paris, France.
[2] Géosciences Azur, CNRS-UNSA, Valbonne, France.
[3] Domaines Océaniques, Institut Universitaire Européen de la Mer, Plouzané, France.

0094-8276/08/2008GL033993$05.00

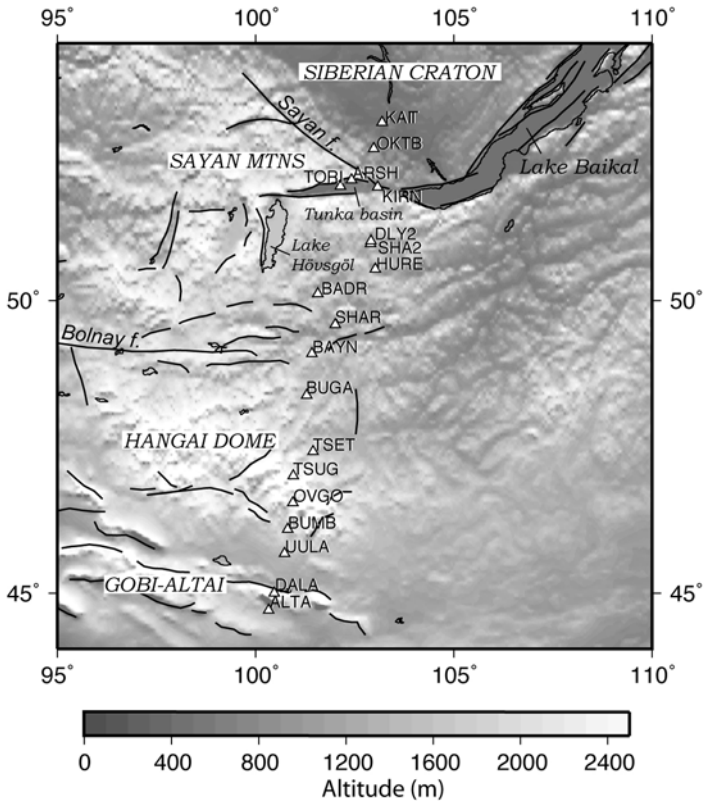

Figure 1. Topography of Western Mongolia and location of the seismological stations of the MOBAL experiment (open triangles). Solid lines are the main active faults (Sayan and Bolnay faults are indicated).

free from common error sources and with a zero average (see, e.g., *Evans and Achauer* [1993] for a review on teleseismic assumptions). These travel time residuals mostly reflect the anomalous velocity patterns compared with the spherical homogeneous IASP91 model. Also comprised in these residuals are the differences coming from the variation of topography between the seismic stations. We thus correct all travel times from the topography effect (assuming a mean upper crust velocity of 5800 m/s) so that they can be all fully comparable only in terms of crust and mantle structures.

3. Topography, Gravity and Traveltime Residuals Inversion

3.1. Method

[7] The largest positive residuals are encountered over the ~3000 m-high Hangai dome, and negative ones over the Siberian craton (Figure 2, top). Traveltime residuals appear positively correlated with the topography with a correlation coefficient of 6.9 (Figure 2, bottom). We interpret velocity variations responsible for the observed travel time residuals as reflecting density contrasts that are echoed in the topographic signal via the isostatic response of the lithosphere. Although we cannot rule out the influence of intra-crustal density variations, these density contrasts should primarily arise from crustal and/or lithospheric thickness variations. Combining travel time residuals with topography variations hence requires an assumption on the mode of isostatic compensation and on the velocity/density conversion factor (B factor of Birch's law [*Birch*, 1961]).

[8] Given the profile length (~1000 km) and the station spacing (50–100 km), it is impossible to distinguish between local and regional isostatic effects, hence we hereafter merely assume a local isostatic compensation. Assuming that teleseismic rays travel almost vertically beneath the stations and contain coherent information for only the first 200–300 km depth [*Evans and Achauer*, 1993], the mean time residual Δt is then proportional to the thickness of low-velocity lower crust and uppermost asthenosphere layers (*Hc* and *Ha*, respectively):

$$\Delta t = Hc\left(\frac{1}{Vc} - \frac{1}{Vm}\right) + Ha\left(\frac{1}{Va} - \frac{1}{Vm}\right) \tag{1}$$

where *Vc*, *Va* and *Vm* are the P-wave velocities of the lower crust, asthenosphere and mantle lithosphere, respectively. In a local isostasy model, the topographic response Δtop to these low-density bodies (crustal root and asthenosphere) is related to *Ha* and *Hc*, with:

$$\Delta top = Hc\left(\frac{\rho m - \rho c}{\rho c}\right) + Ha\left(\frac{\rho m - \rho a}{\rho a}\right) \tag{2}$$

If the *B* factor is identical for the crust, mantle and asthenosphere, then:

$$\frac{\rho m - \rho c}{\rho c} = \frac{Vm - Vc}{Vc} \quad \text{and} \quad \frac{\rho m - \rho a}{\rho a} = \frac{Vm - Va}{Va} \tag{3}$$

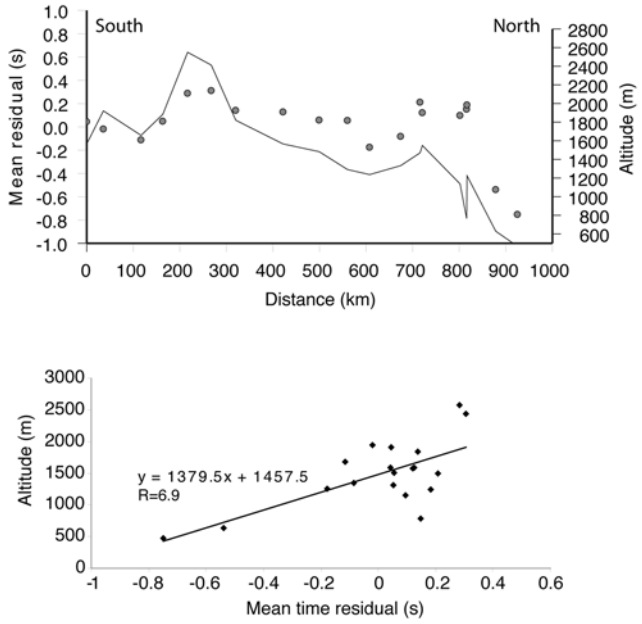

Figure 2. (top) Mean traveltime residuals (left scale, grey dots) and station elevation (right scale, solid line) across the MOBAL profile. (bottom) Correlation between topography and traveltime residuals. The slope should be indicative of the mantle P-wave velocity if the B factor relating velocity with density is constant through the model.

So the mean $\Delta top/\Delta t$ slope should be equal to the velocity of the mantle *Vm* (from equations (1), (2) and (3)). As shown on Figure 2 (bottom), the observed $\Delta top/\Delta t$ slope is only of about 1380 m/s, i.e. ~6 times lower than commonly accepted upper mantle velocities. Consequently, the velocity/density conversion factor could differ between the crust, upper mantle and asthenospheric layers. A small decrease of the B value in the asthenosphere from 2.7 to 2.5 for instance can yield a $\Delta top/\Delta t$ slope reduction of more than 60% if *Ha* = *Hc*, and even more dramatic effects if *Ha* > *Hc*. A possible reason for a lower B value in the asthenosphere could be the presence of partial melting zones causing a decrease of P-wave velocities, and/or a temperature and/or pressure dependence of B factor [e.g., *Christensen and Mooney*, 1995]. We then differ the factor B into crustal (*Bc*), lithospheric mantle (*Bm*) and asthenospheric parts (*Ba*).

[9] The amounts of topography supported by crustal root and asthenospheric uplifting, respectively, are unknown. To avoid a too large number of unconstrained parameters, we assume that the proportion of asthenosphere-supported versus crust-supported topography (*R*) is constant along the profile (*R* = *Ha*/*Hc*). A Monte-Carlo inversion is then performed for the four parameters *Vc*, *Va*, *Ba*, and *R*. At each station, the time residual is used to compute *Hc* and *Ha* (equation (1)) which are then used as inputs for computing the topographic response (equation (2)). The resulting Moho and LAB boundaries with their corresponding density contrasts are then used to compute the Bouguer gravity anomaly. For each set of parameters *Vc*, *Va*, *Ba*, and *R* we computed the Root Mean Square residual (RMS) of the gravity and topography models.

3.2. Results

[10] The range of tested values progressively narrows with the number of iterations depending on the RMS minima of each set of parameters (Figure 3). Each iteration is made up of 3000 trials. The P velocity and B factor are fixed for the mantle part at *Vm* = 8100 m/s and *Bm* = 2.7, respectively. The B factor in the crust is also *Bc* = 2.7. We chose to keep constant and equal B values in the crust and mantle lithosphere since significant variations are more likelyto occur in the asthenosphere because of possible melt zones. Ten iterations are performed (Figure 3). Acceptable B values in the asthenosphere range from 2.3 to 2.8 and this parameter is finally kept fixed at 2.55 after the 3rd iteration. The best fitting models define an asthenosphere velocity slightly lower than 7700 m/s; this parameter is fixed at

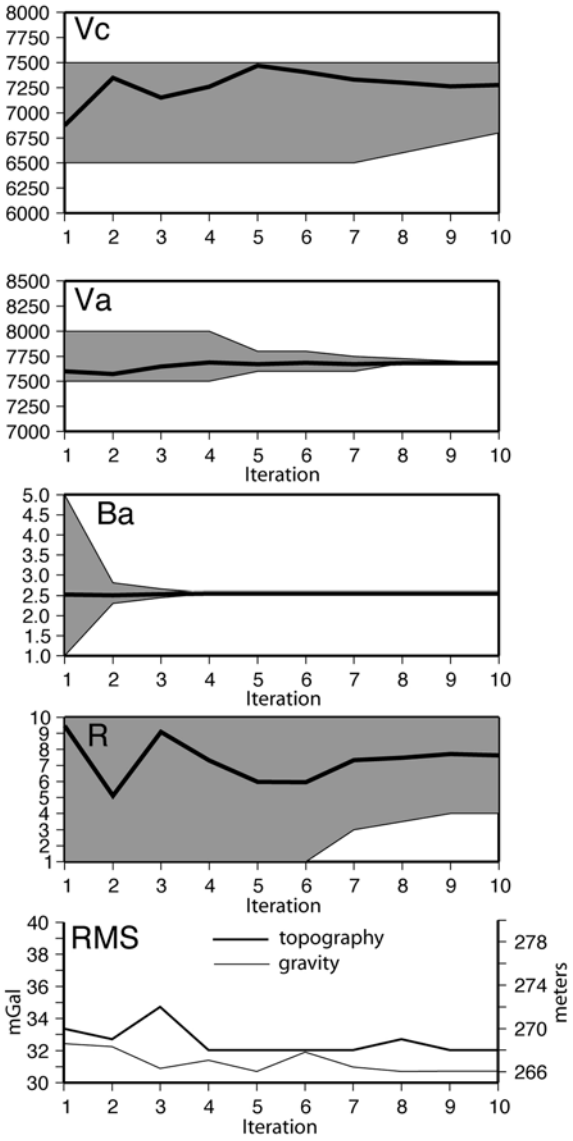

Figure 3. Results of Monte-Carlo inversion showing the range of parameters tested at each iteration (grey polygon) and the best-fitting values (thick lines) for *Vc*, *Va*, *Ba* and *R*, and (bottom) the corresponding RMS for gravity and topography.

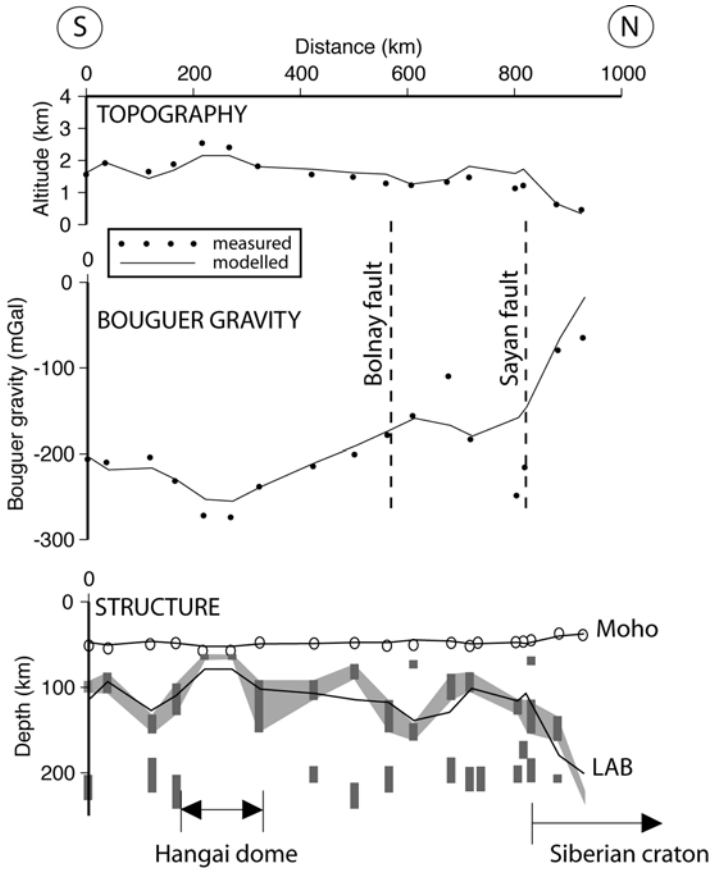

Figure 4. (top) Topography, (middle) gravity and (bottom) lithospheric cross section for the best-fitting model (solid line). Topography and gravity data are solid circles on the top and middle panels. Circles and dark grey bars on the bottom plot correspond to the inferred Moho and to the sub-crustal low-velocity zones depths extracted from the 1D velocity models by *Mordvinova et al.* [2007]. The light grey polygon delineates the position of the inferred lithosphere-asthenosphere boundary from these 1D velocity models.

7680 m/s after the sixth iteration. Clear RMS minima and stable solutions appear for R and Vc only after this step. The best-fitting model yields $Va = 7680$ m/s, $Ba = 2.55$, $Vc = 7277$ m/s and $R = 7.63$. The RMS for Bouguer gravity and topography are of 30.7 mGal and 268 m, respectively. The predicted topography, gravity, and Moho and LAB geometries are shown on Figure 4. The model satisfyingly reproduces the observed topography, although it is slightly too low over the Hangai dome and too high over the Bolnay-Sayan region. The Bouguer gravity is also well explained except close to Bolnay and Sayan faults where observed positive and negative peaks are not reproduced.

3.3. Consistency With Other Models

[11] The predicted asthenosphere and mantle velocities, as well as Moho and LAB depths are compared with the 1D S-wave velocity models obtained from receiver function analyses by *Mordvinova et al.* [2007]. The Moho is easily picked on 1D velocity models as it corresponds to an abrupt downward-positive velocity jump. The position of the LAB is obviously more difficult to infer. We chose to pick the sub-crustal depth intervals where the S-wave velocity significantly decreases. Our model predicts a Moho depth which is in very good agreement with the one deduced from receiver functions, with depths of about 35 km for the two northernmost stations (on the Siberian craton) and ranging between 45 and 54 km for the rest of the profile (Figure 4). The lithosphere-asthenosphere boundary depth inferred from our model is consistent with an alignment of sub-crustal low-velocity zones derived from the S-wave velocity model of *Mordvinova et al.* [2007] (Figure 4). In our model, the lithospheric thickness ranges between 66 km (Hangai) and more than 200 km (Siberian craton). It should be noted however that there is a trade-off between the inverted Moho and LAB depths, as larger Moho depth variations and lower LAB depth variations could account for the observed topography and gravity as well. However, xenolith studies have evidenced that Moho depth beneath Hangai should not be greater than 48–50 km, which precludes that the Hangai dome topography is entirely compensated by crustal thickening [*Ionov*, 2002].

[12] Assuming a mean Vp/Vs ratio of 1.73, the mean velocities in the lowermost crust and at the LAB given by 1D velocity models are of 7411 ± 204 m/s and 7716 ± 127 m/s, respectively, which is consistent with our results. The lower crustal velocity is consistent with a mineral composition typical of mafic garnet granulites [*Christensen and Mooney*, 1995], close to the composition of lower crust xenoliths of the Tariat area, in the Hangai region [*Stosch et al.*, 1995]. Analyses of Tariat mantle xenoliths evidenced a thinned

lithosphere and fertile mantle beneath Hangai, very different from the Siberian craton mantle [*Ionov and Hofmann*, 2007; *Ionov*, 2007]. Our model is globally consistent with this view, though we do not take into account variations in the mantle chemical composition. Finally, our model is consistent with recent regional tomography models of Asia [e.g., *Yanovskaya and Kozhevnikov*, 2003; *Priestley et al.*, 2006]: these models also predict a thick, cold lithosphere down to ~200 km beneath the Siberian craton and a moderately thinned lithosphere beneath central Mongolia.

4. Conclusion

[13] Using simple assumptions on velocity and density structures, we are able to relate travel time residuals and topography correlation with the lithospheric structure beneath the Mongolia-Baikal transect. The long wavelengths of both topography and gravity signal are well retrieved (Figure 4). The corresponding shape of Moho and LAB are consistent with the recent results of *Mordvinova et al.* [2007]. The Moho appears with a relatively flat shape along most of the profile, whereas the LAB exhibits strong variations (between 60 and 200 km depth). The shallower asthenosphere occurs beneath Gobi-Altai Mountains, Hangai Dome and Tunka-Sayan system (Figure 4), where scattered quaternary volcanism is documented [e.g., *Demonterova et al.*, 2007]. The asthenosphere is the deepest in the northern part of the transect which corresponds to the Siberian platform [*Artemieva and Mooney*, 2001].

[14] The discrepancies we observe are very localized and concern short wavelength patterns. In the southern part of the profile, our model underestimates the topography and overestimates the gravity for Hangai Dome (Figure 4). Receiver functions computed for the stations on the Hangai Dome suggest a low velocity layer in the crust that we are unable to retrieve with our model [*Mordvinova et al.*, 2007]. A low-density layer in the crust can create more buoyant material sustaining the topography without any visible effect on travel time residuals, because of the lack of ray crossings at shallow depths. For the northern part of the transect, between Bolnay and Sayan faults, our results differ from those by *Mordvinova et al.* [2007] and our fit to gravity is unsatisfactory for short wavelengths. This difference appears for the location of Sayan and Bolnay active faults, where flexural effects are likely to happen in response to transpressional tectonics taking place along these faults [*Petit et al.*, 2002].

[15] As a consequence, an important part of the topography in central Mongolia is supported by a localised asthenospheric upwelling.

[16] **Acknowledgments.** The authors are grateful to Dickson Cunningham, Fabio Florindo (Editor) and to an anonymous reviewer for their comments on an earlier version of this manuscript. Reviews by Dmitri Ionov and another anonymous reviewer were greatly appreciated.

References

Arjannikova, A., C. Larroque, J.-F. Ritz, J. Déverchère, J.-F. Stéphan, S. Arjannikov, and V. San'kov (2004), Geometry and kinematics of active deformation at the southwesternmost Baikal rift zone (Mongolia-Siberia) from neotectonics and space imagery constraints, *Terra Nova*, *16*, 265–272, doi:10.1111/j.1365-3121.2004.00565.

Artemieva, I., and W. D. Mooney (2001), Thermal thickness and evolution of Precambrian lithosphere: A global study, *J. Geophys. Res.*, *106*, 16,387–16,414.

Birch, F. (1961), The velocity of compressional waves in rocks to 10 kilobars, *J. Geophys. Res.*, *66*, 2199–2224.

Christensen, N. I., and W. D. Mooney (1995), Seismic velocity structure and composition of the continental crust: A global view, *J. Geophys. Res.*, *100*, 9761–9788.

Cunningham, D. (2001), Cenozoic normal faulting and regional doming in the southern Hangay region, Central Mongolia: Implications for the origin of the Baikal Rift Province, *Tectonophysics*, *331*, 389–411.

Cunningham, D. (2005), Active intracontinental transpressional mountain building in the Mongolian Altai: Defining a new class of orogen, *Earth Planet. Sci. Lett.*, *240*, 436–444.

Demonterova, E. I., A. V. Ivanov, S. V. Rasskazov, M. E. Markova, T. A. Yasnygina, and Y. M. Malikh (2007), Lithospheric control on late Cenozoic magmatism at the boundary of the Tuva-Mongolian massif, Khubsugul area, Northern Mongolia, *Petrology*, *15*, 90–107.

Evans, J., and U. Achauer (1993), Teleseismic velocity tomography using the ACH method: Theory and application to continental scale, in *Seismic Tomography: Theory and Practice*, edited by H. Iyer and K. Hirahara, pp. 319–360, CRC Press, Boca Raton, Fla.

Forsyth, D. W. (1985), Subsurface loading and estimates of the flexural rigidity of continental lithosphere, *J. Geophys. Res.*, *90*, 12,623–12,632.

Ionov, D. A. (2002), Mantle structure and rifting processes in the Baikal-Mongolia region: Geophysical data and evidence from xenoliths in volcanic rocks, *Tectonophysics*, *351*, 41–60.

Ionov, D. A. (2007), Compositional variations and heterogeneity in fertile lithospheric mantle: Peridotite xenoliths in basalts from Tariat, Mongolia, *Contrib. Mineral. Petrol.*, *154*, 455–477.

Ionov, D., and A. W. Hofmann (2007), Depth of formation of sub-continental off-craton peridotites, *Earth Planet. Sci. Lett.*, *261*, 620–634.

Kaban, M. K., P. Schwintzer, and C. Reigber (2004), A new isostatic model of the lithosphere and gravity field, *J. Geod.*, *78*, 368–385.

Kennett, B. L. N., and E. R. Engdahl (1991), Traveltimes for global earthquake location and phase identification, *Geophys. J. Int.*, *105*, 429–465.

Missenard, Y., H. Zeyen, D. Frizon de Lamotte, P. Leturmy, C. Petit, M. Sébrier, and O. Saddiqi (2006), Crustal versus asthenospheric origin of the relief of the Atlas Mountains of Morocco, *J. Geophys. Res.*, *111*, B03401, doi:10.1029/2005JB003708.

Mordvinova, V., A. Deschamps, T. Dugarmaa, J. Déverchère, M. Ulzibaat, V. Sankov, A. Artem'ev, and J. Perrot (2007), Velocity structure of the lithosphere on the 2003 Mongolian-Baikal transect from *SV* waves, *Izv. Phys. Solid Earth*, *43*, 119–129.

Petit, C., J. Déverchère, V. San'kov, and D. Fairhead (2002), Deep structure and mechanical behavior of the lithosphere in the Hangai-Hövsgöl region, Mongolia: New constraints from gravity modeling, *Earth Planet. Sci. Lett.*, *197*, 133–149.

Priestley, K., E. Debayle, D. McKenzie, and S. Pilidou (2006), Upper mantle structure of eastern Asia from multimode surface waveform tomography, *J. Geophys. Res.*, *111*, B10304, doi:10.1029/2005JB004082.

Stosch, H. G., D. A. Ionov, I. S. Puchtel, S. J. G. Galer, and A. Sharpouri (1995), Lower crustal xenoliths from Mongolia and their bearing on the nature of the deep crust beneath central Asia, *Lithos*, *36*, 227–242.

Tibéri, C., M. Diament, J. Déverchère, C. Petit, V. Mikhailov, S. Tikhotsky, and U. Achauer (2003), Deep structure of the Baikal rift zone revealed by joint inversion of gravity and seismology, *J. Geophys. Res.*, *108*(B3), 2133, doi:10.1029/2002JB001880.

Vassallo, R., M. Jolivet, J.-F. Ritz, R. Braucher, C. Larroque, C. Sue, M. Todbileg, D. Javkhanbold, and D. L. Bourlès (2007), Uplift age and rates of the Gurvan Bogd system (Gobi-Altay), coupling 10Be and Fission tracks analysis, *Earth Planet. Sci. Lett.*, *259*, 333–346.

Yanovskaya, T. B., and V. M. Kozhevnikov (2003), 3D S-wave velocity pattern in the upper mantle beneath the continent of Asia from Rayleigh wave data, *Phys. Earth Planet. Int.*, *138*, 263–278.

A. Deschamps, Géosciences Azur, CNRS-UNSA, 250 Avenue Albert Einstein, Sophia-Antipolis, F-06560 Valbonne, France.

J. Déverchère, Domaines Océaniques, Institut Universitaire Européen de la Mer, Place Nicolas Copernic, F-29280 Plouzané, France.

C. Petit and C. Tiberi, Laboratoire de Tectonique, CNRS-UPMC, Paris 6, Tour 46-00 E2, boîte 129, 4 Place Jussieu, F-75252 Paris CEDEX, France. (carpetit@ccr.jussieu.fr)